

4-Hz oscillations synchronize prefrontal–amygdala circuits during fear behavior

Nikolaos Karalis^{1–3,6}, Cyril Dejean^{1,2,6}, Fabrice Chaudun^{1,2,6}, Suzana Khoder^{1,2}, Robert R Rozeske^{1,2}, H el ene Wurtz^{1,2}, Sophie Bagur⁴, Karim Benchenane⁴, Anton Sirota³, Julien Courtin^{1,2,5,7} & Cyril Herry^{1,2,7}

Fear expression relies on the coordinated activity of prefrontal and amygdala circuits, yet the mechanisms allowing long-range network synchronization during fear remain unknown. Using a combination of extracellular recordings, pharmacological and optogenetic manipulations, we found that freezing, a behavioral expression of fear, temporally coincided with the development of sustained, internally generated 4-Hz oscillations in prefrontal–amygdala circuits. 4-Hz oscillations predict freezing onset and offset and synchronize prefrontal–amygdala circuits. Optogenetic induction of prefrontal 4-Hz oscillations coordinates prefrontal–amygdala activity and elicits fear behavior. These results unravel a sustained oscillatory mechanism mediating prefrontal–amygdala coupling during fear behavior.

Long-range neuronal synchronization among groups of neurons is an effective mechanism that promotes the transmission of information between neural structures^{1–4}. This form of neuronal communication has been largely described in sensory and motor systems^{5–8} and more recently between neural structures involved in the processing of emotions such as fear-related information^{9–12}. Fear behavior is known to depend on the interaction between the dorsal medial prefrontal cortex (dmPFC) and the basolateral amygdala (BLA), and recent data indicate that local or distant synchronization of neuronal activity in this dmPFC–BLA network strongly correlates with fear behavior^{9–12}. In particular, synchronization of spiking activity between dmPFC and BLA has been associated with resistance to extinction learning, whereas fear discrimination has been associated with transient, sensory-driven dmPFC–BLA synchronization^{10,11}. However, the precise neuronal mechanisms mediating long-range network synchronization during fear behavior remain unknown. Furthermore, a causal role of neuronal synchrony among dmPFC and BLA circuits in driving fear behavior has not yet been demonstrated.

RESULTS

Internally generated freezing behavior

To address these questions, we performed single-unit and local field potential (LFP) recordings in the dmPFC and BLA of freely behaving mice subjected to auditory fear conditioning (Fig. 1a). Twenty-four hours after conditioning, re-exposure to the conditioned auditory stimulus (CS⁺) but not to the control auditory stimulus (CS⁻) induced conditioned freezing behavior, which we used as readout of fear memory acquired upon associative learning (Fig. 1b). Quantification of freezing episodes occurring during or between CS⁺ presentations

indicated that mice froze more often between CS⁺ presentations (Fig. 1c). Moreover, evaluation of freezing-period onset distribution during or between CS⁺ presentations indicated that a large fraction of freezing periods ($41.8 \pm 0.03\%$) were initiated outside of CS⁺ presentations (Fig. 1d). Finally, cross-correlation analysis performed between freezing and CS⁺ onset revealed that the freezing period onset was delayed by 1.5 s with respect to CS⁺ onset (Fig. 1e). These observations indicate, that in addition to freezing episodes driven by auditory inputs, internally generated mechanisms can initiate and maintain freezing episodes following CS⁺ presentations.

dmPFC and BLA 4-Hz oscillations predict freezing behavior

Analysis of dmPFC LFPs recorded throughout the behavioral sessions revealed a prominent and sustained 2–6 Hz oscillation with a peak frequency at 4 Hz (hereafter referred to as 4-Hz oscillations), which strongly correlated with episodes of freezing behavior following conditioning (Fig. 2a–d and Supplementary Fig. 1a,b). These oscillations were not present when animals were passively immobile during the habituation session (Fig. 2a and Fig. 3a–c). Moreover, the duration and power of 4-Hz oscillations in the dmPFC was strongly correlated with the length of freezing episodes (Fig. 3d).

To evaluate whether 4-Hz oscillations could predict freezing behavior, we first computed freezing-triggered spectrograms centered on the onset and offset of freezing episodes (Fig. 3e). Statistical analyses for the temporal progression of significant changes of 4-Hz power indicated that 4-Hz oscillations in the dmPFC emerged and terminated significantly earlier than freezing behavior. These results strongly suggest that 4-Hz oscillations are an accurate predictor of freezing onset and offset, rather than a consequence of freezing

¹INSERM, Neurocentre Magendie, U862, Bordeaux, France. ²Univ. Bordeaux, Neurocentre Magendie, U862, Bordeaux, France. ³Bernstein Center for Computational Neuroscience Munich, Munich Cluster of Systems Neurology (SyNergy), Faculty of Medicine, Ludwig-Maximilians Universit at M unchen, Planegg-Martinsried, Germany. ⁴Team Memory, Oscillations and Brain states (MOBs), Brain Plasticity Unit, CNRS UMR 8249, ESPCI ParisTech, Ecole Sup erieure de Physique et de Chimie Industrielles de la Ville de Paris, Paris, France. ⁵Friedrich Miescher Institute for Biomedical Research, Basel, Switzerland. ⁶These authors contributed equally to this work. ⁷These authors jointly directed this work. Correspondence should be addressed to C.H. (cyril.herry@inserm.fr) or N.K. (karalis@bio.lmu.de).

Received 23 October 2015; accepted 22 January 2016; published online 15 February 2016; doi:10.1038/nn.4251

Figure 1 Freezing behavior is triggered by internally generated mechanisms.

(a) Experimental protocol. Hab., habituation; FC, fear conditioning; Ret., retrieval; US, unconditioned stimulus. (b) Behavioral results.

During habituation, mice ($n = 13$) exhibited low freezing during the CS⁻ and CS⁺. After conditioning (day 2: retrieval), the CS⁺ (CS⁺ 1–12, grouped in blocks of four) induced higher freezing than CS⁻ (paired *t*-tests, CS⁻ versus each CS⁺ block: $t(12) = -11.929$;

$t(12) = -11.929$; $t(12) = -8.442$; all $***P < 0.001$). (c) Percentage of freezing exhibited during and between CS⁺ presentations (paired *t*-test, freezing inside versus between CS⁺: $t(12) = -2.480$, $*P = 0.029$).

(d) Distribution probability for freezing episode duration as a function of whether freezing was initiated inside or between CS⁺ presentations. Inset, percentage of freezing episodes initiated inside or between CS⁺ presentations ($n = 13$ mice, paired *t*-test, $t(12) = 2.762$, $*P = 0.016$).

(e) Cross-correlation analysis performed between freezing and CS⁺ onset ($n = 13$ mice, 100-ms bins). Red vertical dotted line represents freezing onset. Black horizontal dotted line represents significance level. Black arrow indicates the highest probability for CS⁺ onset at 1.5 s before freezing onset. Error bars, mean \pm s.e.m. For box plots, the middle, bottom and top lines correspond to the median, bottom quartile and top quartile, and whiskers to lower and upper extremes minus bottom quartile and top quartile, respectively.

behavior. This observation was further supported by analyses using supervised learning models, which allowed us to successfully predict freezing behavior on a trial-by-trial basis using the 4-Hz dmPFC signal-to-noise ratio (SNR) (Fig. 3f,g). 4-Hz oscillations developed during auditory fear conditioning (Supplementary Fig. 2) and dmPFC 4-Hz oscillations were also observed during freezing episodes in mice submitted to contextual fear conditioning, indicating that 4-Hz oscillations might correspond to a general physiological signature of freezing behavior (Supplementary Fig. 3). A similar but less

prominent phenomenon was observed in the BLA, although the coupling between 4-Hz oscillations and freezing behavior was stronger in the dmPFC, likely because of the different laminar anatomical organization of the two structures and putative localization of the source of the 4-Hz oscillation in the prefrontal circuits (Fig. 4 and Supplementary Figs. 1c,d and 4a–e).

To evaluate whether 4-Hz oscillations were the mere consequence of freezing-, motor- or respiratory-related behavior, we performed further recordings in the ventrolateral periaqueductal gray (vPAG),

Figure 2 Emergence of dmPFC 4-Hz oscillations during freezing behavior. (a) Top, representative dmPFC raw LFP traces recorded during retrieval. 4-Hz oscillatory activity is prominent during freezing behavior. Bottom, representative spectrograms of dmPFC LFPs during habituation and retrieval sessions during CS⁻ and CS⁺ presentations (blue lines, CS⁻ onset; red lines, CS⁺ onset; habituation, recording during CS⁻ 3 and 4; retrieval, recording during CS⁺ 1 and 2). White lines on the spectrogram indicate immobility or freezing episodes.

(b) Representative spectrogram of dmPFC LFPs at a finer time resolution before, during and after presentation of a CS⁺ during retrieval. Each red tick represents a single CS⁺ pip. White lines on the spectrogram indicate freezing episodes. a.u., arbitrary units. (c) Averaged power spectra of dmPFC LFPs recorded during retrieval for freezing and no-freezing periods ($n = 13$ mice). Inset, averaged dmPFC 2–6 Hz power during retrieval for freezing and no-freezing periods (paired *t*-test, freezing versus no freezing: $t(12) = -14.884$, $***P < 0.001$).

(d) Averaged SNR of 4-Hz oscillation (2–6 Hz) during habituation (Hab.) and retrieval (Ret.) ($n = 12$ mice, paired *t*-tests, habituation versus retrieval: dmPFC: $t(11) = -6.805$, $***P < 0.001$). Shaded areas, mean \pm s.e.m. For box plots, the middle, bottom and top lines correspond to the median, bottom quartile and top quartile, and whiskers to lower and upper extremes minus bottom quartile and top quartile, respectively. For representative examples (a,b), similar traces were observed for the 13 animals used in these experiments.

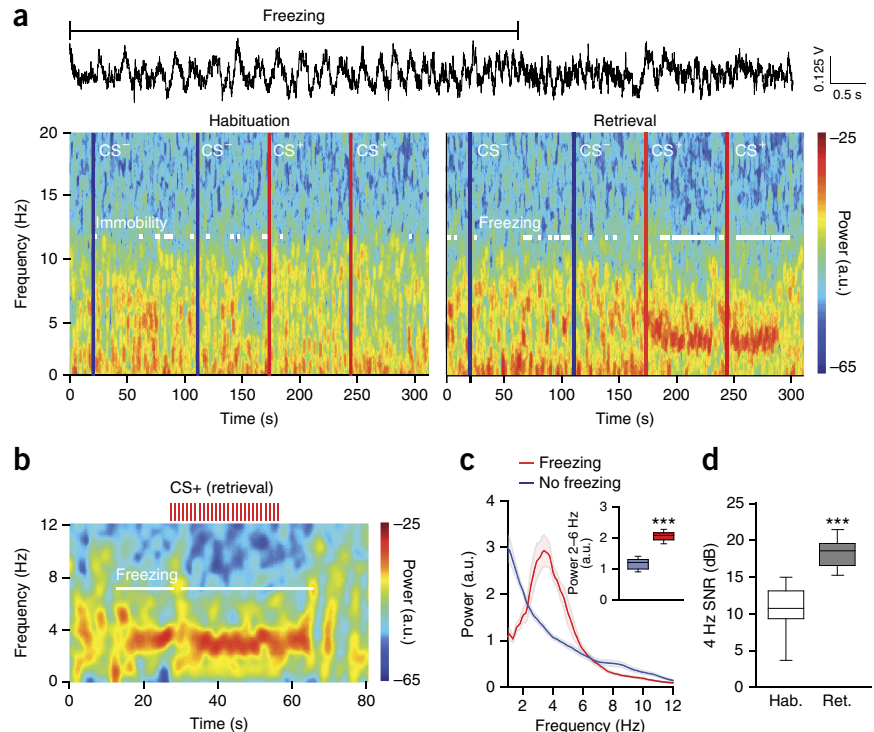
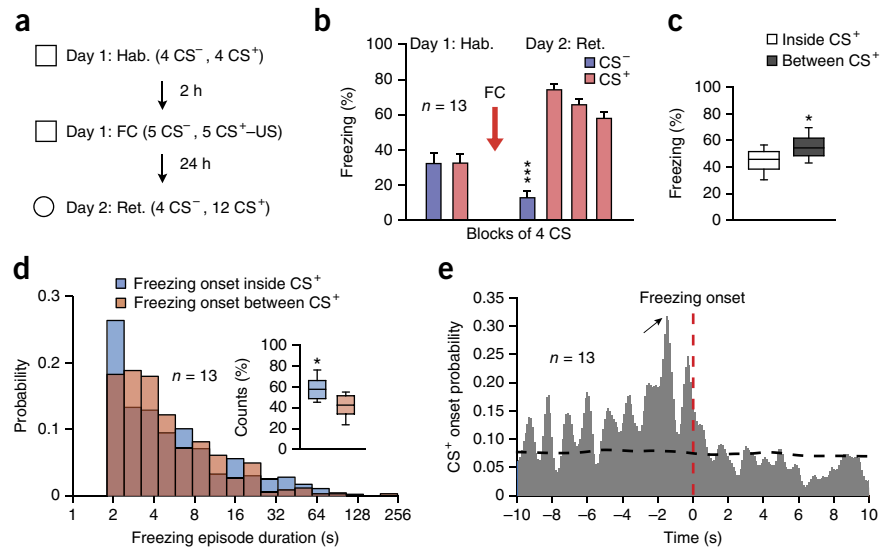
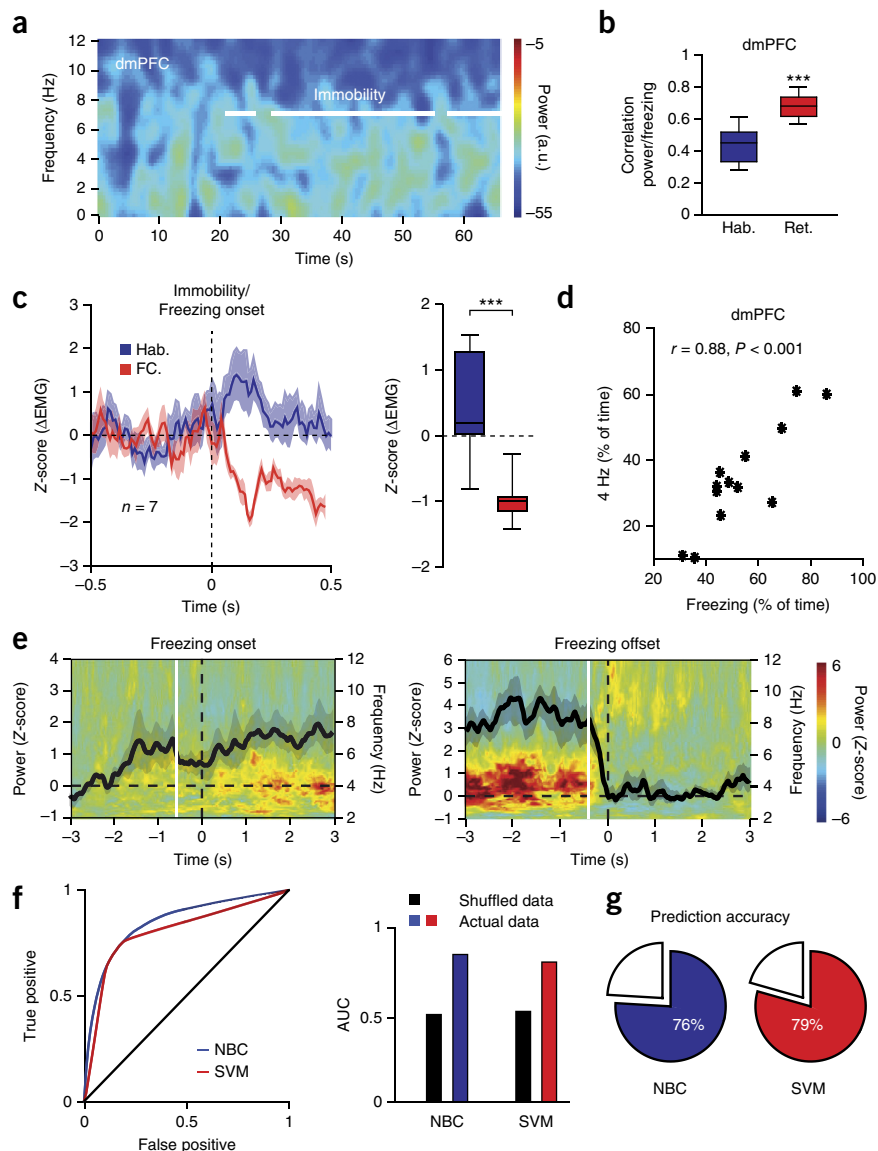


Figure 3 dmPFC 4 Hz oscillations predict freezing. **(a)** Spectrograms of dmPFC LFP during habituation. White lines indicate immobility. **(b)** Correlation between dmPFC 4-Hz power and freezing during habituation and retrieval ($n = 13$ mice, paired t -tests: $t(12) = 6.134$, $***P < 0.001$). **(c)** Left, mean Z-score for neck electromyography (EMG) during immobility or freezing ($n = 7$ mice) for CS⁺ presentations. Right, averaged EMG (0–500 ms after CS⁺, Mann-Whitney U test, habituation (Hab.) versus fear conditioning (FC): $U = 0$, $***P < 0.001$). **(d)** Correlation between freezing and dmPFC 4 Hz ($n = 13$ mice; Pearson's $r = 0.88$, $P < 0.001$). **(e)** Averaged freezing onset-triggered (left) and offset-triggered (right) Z-scored spectrograms of dmPFC LFPs ($n = 13$ mice; black lines, averaged Z-scored power envelope; white lines, first significant bin of 4-Hz power changes (increase, -0.53 ± 0.31 s; decrease, -0.39 ± 0.10 s; one-sample t -test: first significant bin versus hypothetical mean = 0, increase: $t(12) = 19.207$, $P < 0.001$; decrease: $t(12) = 16.615$, $P < 0.001$). **(f)** Left, receiver operating characteristics analysis performed on a naive Bayes classifier (NBC) and support vector machine (SVM) classifier trained on dmPFC 4-Hz SNR during freezing. Right, averaged area under the curve for both classifiers versus shuffled data. **(g)** Accuracy of both classifiers at predicting freezing; a.u., arbitrary units. Power in log scale. Shaded areas, mean \pm s.e.m. For box plots, the middle, bottom and top lines correspond to the median, bottom quartile and top quartile, and whiskers to lower and upper extremes minus bottom quartile and top quartile, respectively. For the representative example in **a**, similar traces were observed for the 13 animals used in these experiments.

a neuronal structure involved in the genesis of freezing behavior and the control of breathing during emotional load^{13–16}. Power spectrum analyses performed on vPAG recordings did not reveal significant 4-Hz oscillations during freezing episodes, which strongly suggests that 4-Hz oscillations do not reflect freezing-, motor- or respiratory-related activity (**Supplementary Fig. 4f,g**).

4-Hz oscillations are distinct from theta oscillations

To evaluate whether dmPFC 4-Hz oscillations could correspond to hippocampus-dependent low theta oscillations observed previously during conditioned stimulus presentations^{10,12,17,18}, we inactivated the medial septum, a neuronal structure known to be involved in the genesis of theta oscillations¹⁹. Targeted, reversible inactivation of the medial septum with muscimol, which is known to reduce theta power in the dorsal hippocampus¹⁹, impaired dmPFC theta but had no effect on dmPFC 4-Hz oscillations (**Supplementary Fig. 5a–e**). In addition, this manipulation had no effects on the percentage of dmPFC neurons phase-locked to 4-Hz oscillations but reduced the number of dmPFC neurons phase-locked to theta oscillations (**Supplementary Fig. 5f**). Furthermore, in contrast to transient dmPFC local theta oscillations, which displayed CS⁺-evoked phase resetting and were short-lasting (~ 300 ms)^{9,10}, the sustained dmPFC 4-Hz oscillations were not modulated by CS⁺ presentations, did not display CS⁺-evoked phase resetting (**Supplementary Fig. 6**) and could be maintained

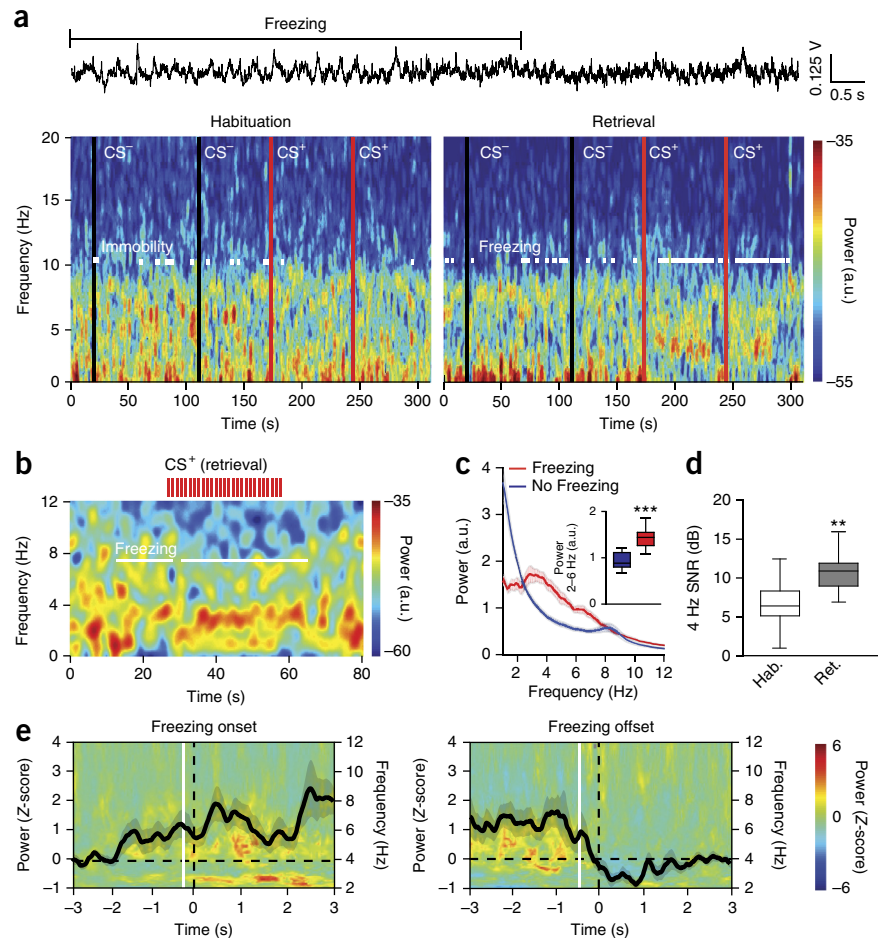


over long periods of freezing behavior even between CS⁺ presentations (**Figs. 2a,b, 3d** and **4a,b**), suggesting that the two phenomena are generated independently. Together these data indicate that the development of hippocampus-independent, internally generated 4-Hz oscillations in dmPFC–BLA circuits precede and therefore predict freezing behavior.

dmPFC 4-Hz oscillations drive BLA during freezing

Analyses of moment-to-moment covariations in oscillatory power and phase between structures revealed that during freezing episodes 4-Hz oscillations in the dmPFC and BLA were strongly synchronized (**Fig. 5a,b** and **Supplementary Fig. 7**). Consequently, coherence between dmPFC and BLA LFPs was significantly enhanced during freezing behavior (**Fig. 5c** and **Supplementary Fig. 7**). Moreover, a series of statistical directionality measures, in both the phase and the amplitude domains, revealed that dmPFC 4-Hz oscillations led BLA LFPs during freezing episodes but not during locomotor activity (**Fig. 5b–d** and **Supplementary Fig. 7**). Together, these data demonstrate that conditioned freezing behavior is associated with a preferential dmPFC-to-BLA phase coupling of 4-Hz LFP oscillations.

Figure 4 BLA 4-Hz oscillations emerge during freezing. **(a)** Top, representative BLA LFP traces recorded during retrieval. Bottom, spectrograms of BLA LFPs during habituation and retrieval during CS⁻ and CS⁺ (black lines, CS⁻ onset; red lines, CS⁺ onset). White lines indicate immobility or freezing. **(b)** Spectrogram of BLA LFPs before, during and after presentation of a CS⁺ during retrieval. Red ticks represent single CS⁺ pips. White lines indicate freezing. **(c)** Averaged power spectrum of BLA LFPs recorded during retrieval for freezing and no freezing ($n = 13$ mice). Inset, averaged BLA 2–6 Hz power during retrieval for freezing and no freezing (paired t -test, freezing versus no freezing: $t(12) = 6.077$, $***P < 0.001$). **(d)** Averaged 4-Hz SNR during habituation (Hab.) and retrieval (Ret.) ($n = 12$ mice, paired t -tests, habituation versus retrieval: BLA, $t(11) = 3.334$, $**P = 0.003$). **(e)** Averaged freezing onset-triggered (left) and offset-triggered (right) Z-scored spectrograms of BLA LFPs ($n = 13$ mice; black lines, averaged Z-scored power envelope; white lines, first significant bin of 4-Hz power changes (increase, -0.27 ± 0.20 s; decrease, -0.46 ± 0.22 s; one-sample t -test: first significant bin versus hypothetical mean = 0, increase: $t(12) = 10.976$, $P < 0.001$; decrease: $t(12) = 34.372$, $P < 0.001$); a.u., arbitrary units. Spectral power in log scale. Shaded areas, mean \pm s.e.m. For box plots, the middle, bottom and top lines correspond to the median, bottom and top quartile, and whiskers to lower and upper extremes minus bottom quartile and top quartile, respectively. For representative examples **(a,b)**, similar traces were observed for the 13 animals used in these experiments.



4-Hz oscillations organize dmPFC and BLA firing activity

To evaluate the consequences of synchronized 4-Hz oscillatory activity for individual dmPFC and BLA putative excitatory principal neurons ($n = 92$ and $n = 72$, respectively) and putative inhibitory interneurons ($n = 35$ and $n = 15$, respectively) (Supplementary Fig. 8), we measured the phase-locking to dmPFC 4-Hz oscillations and changes in firing frequency of dmPFC and BLA neurons during fear behavior. These analyses revealed that a large proportion of principal neurons and interneurons in both structures were significantly phase-locked to dmPFC 4-Hz oscillations during freezing episodes, among which the vast majority exhibited 4-Hz-related oscillatory activity (Fig. 6). Moreover, freezing episodes were associated with a global increase in the firing rate of principal neurons compared to the rate during no-freezing periods in both the dmPFC and the BLA (Supplementary Fig. 8). Correlation and co-firing analyses of pairwise spiking activity performed between neurons recorded in the dmPFC and neurons recorded in the BLA indicated that phase-locked pairs of principal neurons were more co-activated during freezing episodes as compared to both no-freezing periods and non-phase-locked neurons (Fig. 6c,h). Together, these data indicate that dmPFC and BLA principal neurons synchronize their firing activity to 4-Hz oscillations during freezing behavior.

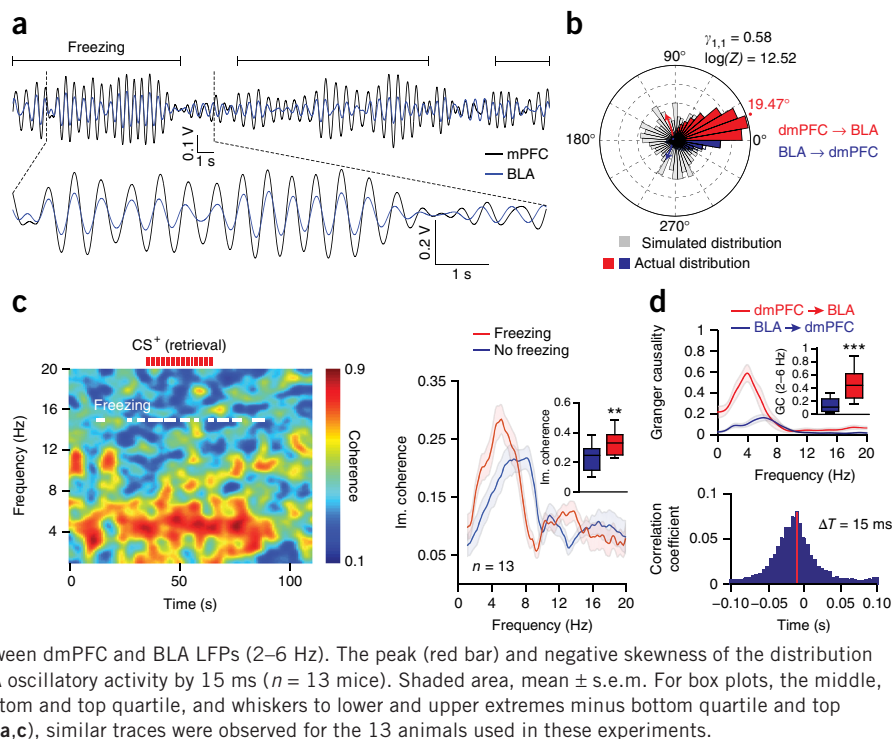
Optogenetic induction of dmPFC 4 Hz drives fear behavior

To further evaluate the causal role of 4-Hz oscillations in synchronizing dmPFC–BLA principal neurons firing activity during fear behavior, we artificially induced 4-Hz oscillations in the dmPFC

of naive animals by analog optogenetic modulation of dmPFC interneurons, which contribute to the emergence of dmPFC 4-Hz oscillations (Supplementary Fig. 9). In particular, we manipulated parvalbumin-expressing cells, which is an efficient approach for inducing rhythmic inhibition of cortical principal neurons at low frequencies^{20–22}. These genetically identified cells were predominantly phase-locked to 4-Hz oscillations and displayed 4-Hz oscillatory activity (Supplementary Fig. 9d–j). Rhythmically driving parvalbumin-expressing interneurons at 4 Hz resulted in prominent 2–6 Hz oscillations in the dmPFC and induced persistent fear behavior (Fig. 7a–c and Supplementary Fig. 10a,b). Freezing behavior was frequency and structure specific, as dmPFC rhythmic stimulation using a number of different control frequencies and BLA or motor cortex stimulation at 4 Hz were inefficient at inducing fear responses (Fig. 7d,e and Supplementary Fig. 10c,d). Furthermore, the artificial induction of dmPFC 4-Hz oscillations synchronized dmPFC and BLA spiking activity during freezing episodes (Fig. 7f and Supplementary Fig. 10g–i).

Given the emergence of 4-Hz oscillations during fear conditioning and retrieval of contextual fear memory (Supplementary Figs. 2 and 3), we retested the mice 24 h later in the context in which they received artificial induction of 4-Hz oscillations. In these conditions, mice exhibited more contextual fear behavior than GFP control animals (Fig. 7c and Supplementary Fig. 10a,b). Furthermore, mice exhibited low freezing levels when tested in a neutral context 24 h later, indicating that fear behavior was specific to the context where the optogenetic stimulation occurred (Supplementary Fig. 10b).

Figure 5 Synchronization of dmPFC and BLA 4-Hz oscillations during freezing. (a) Overlaid filtered (2–6 Hz) dmPFC and BLA LFP traces illustrating synchronized 4 Hz during freezing. (b) Circular distribution of the phase differences between dmPFC and BLA LFPs recorded for freezing during retrieval compared to a control bootstrap-simulated phase distribution ($n = 13$ mice). (c) Left, representative coherogram for dmPFC and BLA LFPs recorded during retrieval during CS⁺. Red ticks represent individual CS⁺ pips. White lines indicate freezing. Right, averaged dmPFC and BLA LFPs imaginary coherence (Im. coherence) for freezing and no freezing during retrieval (paired t -test, freezing versus no freezing: $t(12) = 3.933$, $**P = 0.002$). (d) Top, Granger causality (GC) analysis performed between dmPFC and BLA LFPs during freezing (retrieval, paired t -test, dmPFC \rightarrow BLA versus BLA \rightarrow dmPFC: $t(12) = -5.940$, $***P < 0.001$). Bottom, averaged cross-correlogram performed between dmPFC and BLA LFPs (2–6 Hz). The peak (red bar) and negative skewness of the distribution indicate that dmPFC 4-Hz oscillations lead the BLA oscillatory activity by 15 ms ($n = 13$ mice). Shaded area, mean \pm s.e.m. For box plots, the middle, bottom and top lines correspond to the median, bottom and top quartile, and whiskers to lower and upper extremes minus bottom quartile and top quartile, respectively. For representative examples (a,c), similar traces were observed for the 13 animals used in these experiments.



Together, these results indicate that freezing behavior upon artificial induction of dmPFC 4-Hz oscillations cannot be explained by motor impairments and further suggest that 4-Hz oscillations are causally involved in the synchronization of dmPFC–BLA spiking activity and the expression of aversive fear memories. Finally, post-training optogenetic silencing of BLA neurons during CS⁺ presentations reduced fear behavior, indicating that the BLA is necessary for the full expression of conditioned fear behavior (Supplementary Fig. 10e,f).

DISCUSSION

In this study, we demonstrated that expression of conditioned fear memories is associated with prominent synchronous 4-Hz oscillations in dmPFC–BLA circuits, which organize the spiking activity of local neuronal populations. Furthermore, both dmPFC and BLA 4-Hz oscillations develop specifically during fear conditioning and predict the onset and offset of freezing episodes. The length of freezing episodes was also strongly correlated with the duration and power of dmPFC 4-Hz oscillations, a phenomenon not observed in the BLA. This could be due to the different laminar anatomical organization of the two structures. Aligned pyramidal cells in the cortex form spatially coherent dipoles. The resulting summation of field potentials allows the detection of high-SNR oscillations in the extracellular space²³. The BLA, by contrast, is a nuclear structure with no clear anatomical organization (dipoles are distributed uniformly and not aligned). Consequently, the SNR of extracellularly recorded LFP oscillations is expected to be lower than in the dmPFC. Nonetheless, spike trains of a number of BLA neurons present both intrinsic 4-Hz oscillations and phase-locking to dmPFC 4 Hz, whether under physiological conditions or during light stimulation. Moreover, the presence of 4-Hz oscillations in LFP is indicative of the underlying synaptic activity; however, differences in the absolute power to SNR ratio between the two structures cannot be interpreted as a stronger involvement of the dmPFC. Again, because of the radically different neuronal organization between the two structures, synaptic

inputs are differentially filtered by the biophysical properties of the BLA neural tissue^{24,25}.

Our data indicate that internally generated freezing-related 4-Hz dmPFC oscillations constitute a specific oscillatory mechanism, distinct from the CS⁺-evoked dmPFC theta resetting observed previously^{9,10,12}. These previously published studies^{9,10} evaluated transient sensory-evoked theta oscillations in the dmPFC, which lasted around 300 ms and have been linked to sensory-driven processes during fear behavior or fear discrimination^{9,10}. In contrast, the 4-Hz oscillatory phenomenon correlated not only with long periods of freezing behavior observed during CS⁺ presentations, but also with spontaneously occurring freezing episodes. Functionally this implies that spontaneously occurring freezing periods are internally maintained or generated and not directly driven by sensory stimulations. To our knowledge, this is the first report of a sustained brain state (4-Hz oscillations) that predicts and temporally coincides with freezing episodes. The freezing responses observed between CS presentations are unlikely to have been triggered by the context for several reasons. First, mice were tested in a context distinct from the one used for the conditioning session. Second, freezing levels during CS⁻ presentations during retrieval were very low, indicating that the retrieval context was not aversive *per se* (Fig. 1b; 13.19% freezing on CS⁻ presentations). Our interpretation that freezing episodes occur between CS presentations relies on the induction of a fearful state after the initial CS-induced retrieval of the fear memory and thus the emergence of non-CS-related spontaneous freezing episodes.

Our data and analyses suggest that the 4-Hz oscillations represent a mechanism for the initiation and maintenance of freezing episodes, inside and outside of CS presentations. The data also confirm published observations that CS⁺ onset is associated with a transient resetting of the phase of theta oscillations^{9,10}, which is, however, specific for oscillations in the 8–12 Hz range and is associated with transient increases in theta power, but is not observed for the 4-Hz oscillations (Supplementary Fig. 6). Hence, these observations

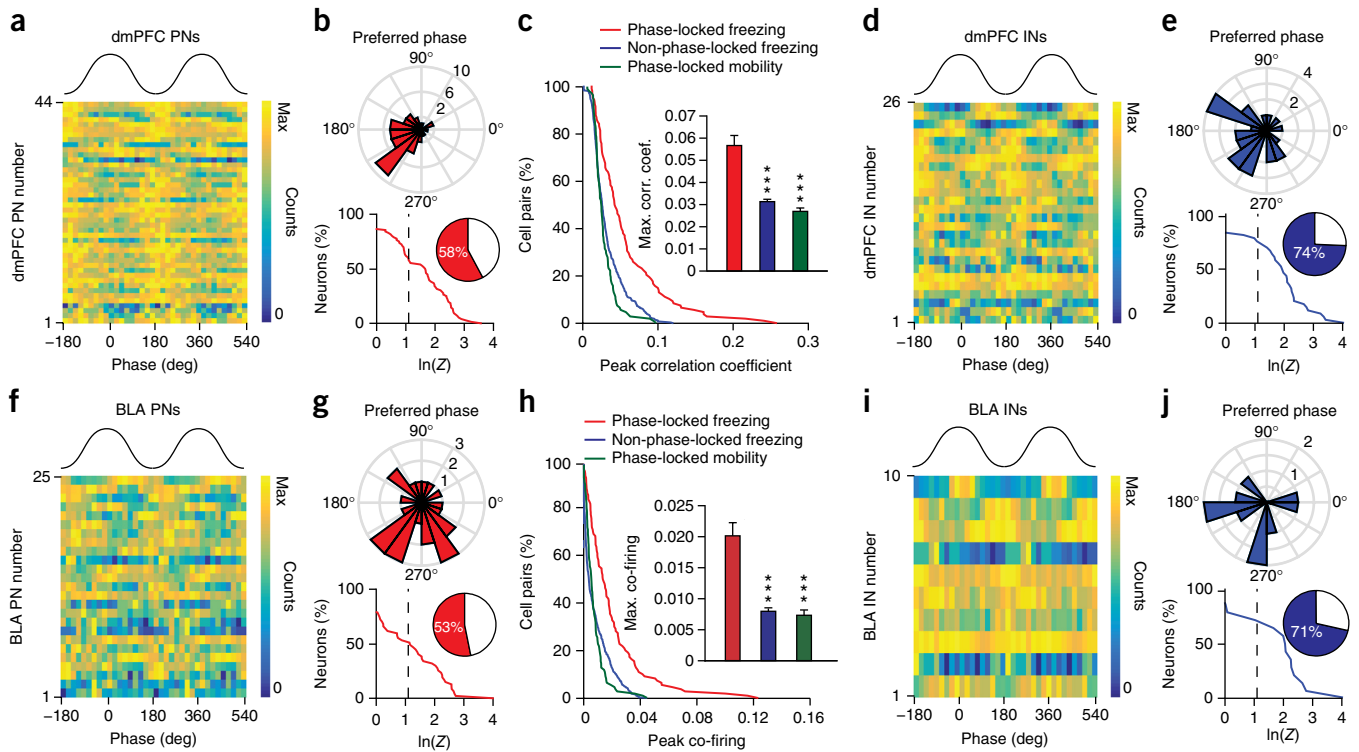


Figure 6 4-Hz oscillations synchronize dmPFC–BLA spiking activity. (**a,d,f,i**) Phase distribution relative to 4-Hz oscillations for dmPFC (**a,d**) and BLA (**f,i**) putative excitatory principal neurons (PN) (**a,f**) or putative inhibitory interneurons (IN) (**d,i**). (**b,g,e,j**) Circular distribution of the 4-Hz preferred phase for populations of dmPFC (**b,e**, top) and BLA (**g,j**, top) phase-locked PNs (**b,g**) and INs (**e,j**) during freezing (dmPFC: 44 PNs and 26 INs; BLA: 25 PNs and 10 INs) and cumulative distribution of log-transformed Rayleigh's test Z of dmPFC (**b,e**, bottom) and BLA (**g,j**, bottom) PNs (**b,g**) and INs (**e,j**). Inset, percentage of dmPFC and BLA neurons significantly phase-locked to 4-Hz oscillations. Dashed line, significant 4-Hz phase-locking threshold ($\ln(Z) = 1.097$, $*P < 0.05$, dmPFC: 44 of 92 PNs and 26 of 35 INs; BLA: 25 of 72 PNs and 10 of 15 INs). (**c,h**) Cumulative distribution of peak correlation coefficient (**c**) and co-firing index (**h**) for pairs of dmPFC and BLA phase-locked and non-phase-locked neurons during freezing and mobility. Insets, maximum correlation coefficient (**c**) and co-firing index (**h**) for all pairs of recorded dmPFC and BLA neurons (phase-locked pairs, $n = 180$; non-phase-locked pairs, $n = 911$; Mann-Whitney U test, top and bottom, phase-locked pairs during freezing versus mobility or non-phase-locked pairs: $U = 50,313, 7,893, 16,200, 9,413$, $**P < 0.001$, $***P < 0.001$). Error bars, mean \pm s.e.m.

indicate that sustained 4-Hz oscillations described in the present manuscript do not correspond to sensory-driven transient theta oscillations previously observed^{9,10}. Taken together, these results have important functional consequences, as they indicate the existence of distinct and independent dmPFC neuronal oscillations involved in the regulation of different aspects of fear behavior, such as stimulus-evoked attention processes related to the presentation of a salient CS, fear discrimination or the expression of freezing behavior. Notably, all of these findings were observed in mice, further studies are required to evaluate whether these oscillations also occurs in different species.

Our data also indicate that stationary dmPFC 4-Hz oscillations do not correspond to hippocampus-mediated dmPFC theta oscillations observed previously¹⁷, as muscimol inactivation of the medial septum blocked hippocampal theta recorded in the dmPFC without affecting prefrontal 4-Hz oscillations, nor the percentage of dmPFC neurons phase-locked to 4-Hz oscillations. Our observation of BLA 4-Hz oscillatory activity during freezing behavior is consistent with previous recordings of slow theta oscillations in the lateral amygdala during fear behavior, which correlate with dorsal hippocampal theta oscillations^{17,18}, although in these studies the temporal relation between CS⁺ onset, 4-Hz oscillatory activity and freezing onset and offset were not clearly established. A recent observation of power increase for 4–7.5 Hz oscillations in the cingulate cortex during a hippocampus-dependent trace fear-conditioning procedure is also partly consistent with our observation²⁶. Indeed, the authors observed

that in some conditioning trials, 4–7.5 Hz power increased during the interval separating the conditioned stimulus from the footshock. In that study, however, the neuronal interaction between the cingulate cortex and the BLA, the precise temporal relation between slow oscillation and freezing behavior, and the causal role of prefrontal 4-Hz oscillations were not established. These data nevertheless suggest that prefrontal 4-Hz oscillations might be a general mechanism of fear expression encompassing classical auditory and contextual fear conditioning.

A key finding of our study comes from the demonstration that, during freezing behavior, dmPFC 4-Hz oscillations entrain BLA oscillatory activity and synchronize spiking activity between dmPFC and BLA neurons. Recent publications have highlighted neuronal co-firing between prefrontal cortex and amygdala during resistance to extinction behavior¹¹, LFP coherence between dmPFC and BLA after CS⁺ onset during fear discrimination, and amygdala neurons phase-locked to dmPFC theta oscillations during fear discrimination¹⁰. To our knowledge, our data provide the first mechanistic demonstration of a 4-Hz-mediated long-range synchronization of spiking activity between dmPFC and BLA during freezing behavior. Moreover, our findings also indicate that dmPFC activity leads the BLA one during freezing behavior.

Accordingly, we found that the optogenetically mediated artificial induction of 4-Hz oscillations in dmPFC synchronizes dmPFC and BLA neuronal activity and increases freezing behavior in a persistent manner, which demonstrates that internally generated

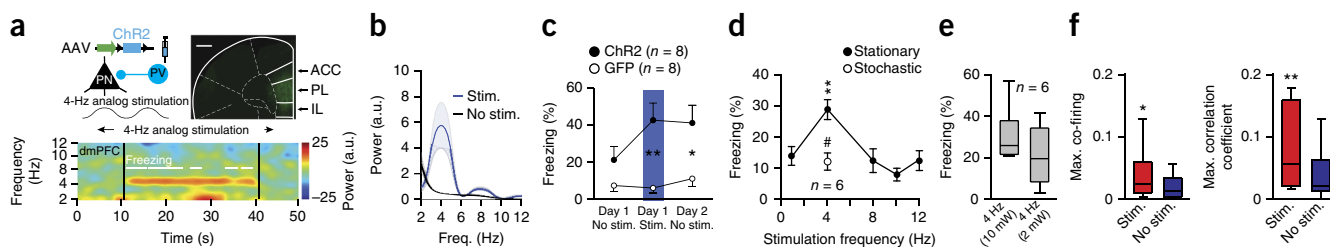


Figure 7 Optogenetic induction of dmPFC 4-Hz oscillations drives freezing. **(a)** Top left, strategy used to activate parvalbumin-expressing (PV) interneurons. Top right, coronal dmPFC micrograph from a PV-IRES-Cre mouse expressing channelrhodopsin2 (ChR2). Solid and dashed lines represent the boundaries between the cingulate cortex (ACC), the prelimbic (PL) and infralimbic (IL) areas, and other cortical structures. Scale bar, 0.5 mm. Bottom, spectrogram during 4-Hz analog stimulation. **(b)** Averaged normalized LFP power spectra of dmPFC LFPs during (Stim.) and outside (No stim.) stimulation ($n = 8$). **(c)** Percentage of freezing for ChR2 ($n = 8$) or GFP ($n = 8$) mice before, during and after 4-Hz induction (two-way ANOVA repeated measures; group: $F(1,14) = 0.868$, $P = 0.367$, time $F(1,2) = 8.926$, $P = 0.001$, group \times time $F(1,28) = 6.925$, $P = 0.0036$); unpaired t -tests: day 1: Stim. $t(14) = 3.712$, $**P = 0.002$; day 2: No stim., $t(14) = 2.758$, $*P = 0.013$). **(d)** Percentage of freezing for ChR2 mice ($n = 6$) during analog stimulation at 1, 4, 8, 10, 12 Hz (Stationary) or using a 4-Hz stochastic waveform (stationary: one-way repeated measures ANOVA: $F(5,4) = 8.618$, $P < 0.001$; Bonferroni-corrected paired t -tests: 4 versus 1 Hz: $t(5) = 5.927$, $**P = 0.0019$; 4 versus 8 Hz: $t(5) = 4.712$, $**P = 0.0053$; 4 versus 10 Hz: $t(5) = 7.632$, $***P < 0.001$; 4 versus 12 Hz: $t(5) = 4.009$, $**P = 0.01$; paired t -test: 4-Hz stationary versus stochastic: $t(5) = 3.533$, $\#P < 0.016$). **(e)** Percentage of freezing for ChR2 ($n = 6$) mice during dmPFC 4-Hz analog stimulation at 2 or 10 mW (paired t -test: $t(5) = 0.951$, $P = 0.385$). **(f)** Maximum correlation and co-firing index for pairs of dmPFC and BLA neurons during and outside stimulation ($n = 31$ pairs, Mann-Whitney, $U = 326$ and 278 , $*P = 0.03$; $**P = 0.004$). a.u., arbitrary units. Power in log scale. Shaded area and error bars, mean \pm s.e.m. For box plots, the middle, bottom and top lines correspond to the median, bottom and top quartiles, and whiskers to lower and upper extremes minus bottom quartile and top quartile, respectively. For representative examples **(a)**, similar images and traces were observed for the 16 (top, 8 ChR2 and 8 GFP mice) and 8 (bottom, 8 ChR2 mice) animals used in these experiments.

oscillations drive behavior. Neuronal synchronization between dmPFC and BLA has been classically evaluated using powerful correlational analyses^{10,11,18}, but never causally demonstrated. Our data indicate that the genesis of 4-Hz oscillations in the dmPFC is sufficient to synchronize neuronal activity between dmPFC and BLA and further drive the expression of freezing responses. Moreover, this effect was frequency and structure specific, as dmPFC manipulation at other frequencies or 4-Hz induction in the motor cortex and BLA did not induce any behavioral effects. However, our data indicate that when freezing behavior is induced following auditory fear conditioning, the BLA is necessary for its full expression. Together these data strongly suggest that dmPFC 4-Hz oscillations are instrumental for dmPFC–BLA synchronization of neuronal activities during fear behavior and that the synchronized firing activity of BLA neurons triggers fear responses (**Supplementary Fig. 11**).

The dmPFC 4-Hz analog optogenetic stimulation induced freezing behavior not only during the stimulation but also 24 h later in the context in which the mice were stimulated. This observation suggests that the artificial induction of dmPFC 4-Hz oscillations might be involved in the formation of associative fear memories. Another possibility could be that this artificial induction might lead to nonspecific anxiety behavior. However, it is unlikely that a sudden inactivation or rhythmic inhibition of prefrontal areas could lead to nonspecific anxiety behavior for at least two reasons. Optogenetic inactivation of the cingulate cortex during remote contextual memory retrieval results in a reduction of contextual fear behavior, an observation not consistent with a general increase in anxiety levels²⁷. Furthermore, in our optogenetic experiments (**Fig. 7**), dmPFC 4-Hz induction induced freezing in a context-specific manner, which is also an observation not consistent with a general increase in anxiety. Furthermore, while it is possible that induction of 4-Hz oscillations leads to the formation of associative fear memories, an alternative interpretation is that the contextual fear memory observed 24 h after optogenetic stimulation is a direct consequence of the association between contextual elements and the aversive state induced by 4-Hz oscillations. This interpretation is consistent with the notion that dmPFC–BLA 4-Hz oscillations are causally involved in the expression of freezing behavior.

Although our data indicate that dmPFC 4-Hz oscillations are causally involved in the neuronal synchronization of spiking activity between dmPFC and BLA during freezing behavior, it is conceivable that this mechanism could be involved in other emotional processes, such as avoidance, flight responses, sensory processes or cognitive tasks. For instance, recent reports have observed 4-Hz oscillations in the whisker barrel cortex during respiration²⁸ and in the rat dmPFC under working memory load during locomotor behavior²⁹. Another important question is the source of the 4-Hz oscillations. Although our data indicate that these oscillations do not originate from the hippocampus and are localized in dmPFC circuits, more work will be required to address this question and unequivocally identify the source of the 4-Hz oscillations. In summary, our data reveal a specific 4-Hz oscillatory mechanism allowing the expression of fear memories by long-range synchronization of neuronal activity between dmPFC and BLA neuronal circuits.

METHODS

Methods and any associated references are available in the [online version of the paper](#).

Note: Any Supplementary Information and Source Data files are available in the online version of the paper.

ACKNOWLEDGMENTS

We thank the members of the Herry laboratory for discussions and comments on the manuscript and K. Deisseroth (Stanford University) and E. Boyden (Massachusetts Institute of Technology) for generously sharing material. This work was supported by grants from the French National Research Agency (ANR-2010-BLAN-1442-01; ANR-10-EQPX-08 OPTOPATH; LABEX BRAIN ANR 10-LABX-43, LABEX TRAIL ANR 10-LABX-57), the European Research Council (ERC) under the European Union's Seventh Framework Program (FP7/2007-2013)/ERC grant agreement no. 281168, the Conseil Régional d'Aquitaine (C.H.), the Fondation pour la Recherche Médicale (FRM) (F.C.), the CNRS ATIP program (2014) and the city of Paris (Grant Emergence 2014), the French National Research Agency (ANR-10-LABX-54 MEMO LIFE; ANR-11-IDEX-0001-02 PSL) (K.B.), Munich Cluster for Systems Neurology (SyNergy, EXC 1010), Deutsche Forschungsgemeinschaft Priority Program 1665 and 1392 and Bundesministerium für Bildung und Forschung via grant no. 01GQ0440 (Bernstein Centre for Computational Neuroscience Munich) (A.S.) and a scholarship from the Erasmus Mundus program Neurasmus (N.K.).

AUTHOR CONTRIBUTIONS

S.B., K.B., F.C., J.C., C.D., N.K., S.K., R.R.R., A.S. and H.W. performed the experiments and analyzed the data. J.C., C.D., N.K. and C.H. designed the experiments. C.H. wrote the paper.

COMPETING FINANCIAL INTERESTS

The authors declare no competing financial interests.

Reprints and permissions information is available online at <http://www.nature.com/reprints/index.html>.

- Bosman, C.A. *et al.* Attentional stimulus selection through selective synchronization between monkey visual areas. *Neuron* **75**, 875–888 (2012).
- Siegel, M., Donner, T.H., Oostenveld, R., Fries, P. & Engel, A.K. Neuronal synchronization along the dorsal visual pathway reflects the focus of spatial attention. *Neuron* **60**, 709–719 (2008).
- Rodriguez, E. *et al.* Perception's shadow: long-distance synchronization of human brain activity. *Nature* **397**, 430–433 (1999).
- Hipp, J.F., Engel, A.K. & Siegel, M. Oscillatory synchronization in large-scale cortical networks predicts perception. *Neuron* **69**, 387–396 (2011).
- Friedrich, R.W., Habermann, C.J. & Laurent, G. Multiplexing using synchrony in the zebrafish olfactory bulb. *Nat. Neurosci.* **7**, 862–871 (2004).
- Riehle, A., Grün, S., Diesmann, M. & Aertsen, A. Spike synchronization and rate modulation differentially involved in motor cortical function. *Science* **278**, 1950–1953 (1997).
- Benchenane, K. *et al.* Coherent theta oscillations and reorganization of spike timing in the hippocampal–prefrontal network upon learning. *Neuron* **66**, 921–936 (2010).
- Gregoriou, G.G., Gotts, S.J., Zhou, H. & Desimone, R. High-frequency, long-range coupling between prefrontal and visual cortex during attention. *Science* **324**, 1207–1210 (2009).
- Courtin, J. *et al.* Prefrontal parvalbumin interneurons shape neuronal activity to drive fear expression. *Nature* **505**, 92–96 (2014).
- Likhtik, E., Stujenske, J.M., Topiwala, M.A., Harris, A.Z. & Gordon, J.A. Prefrontal entrainment of amygdala activity signals safety in learned fear and innate anxiety. *Nat. Neurosci.* **17**, 106–113 (2014).
- Livneh, U. & Paz, R. Amygdala-prefrontal synchronization underlies resistance to extinction of aversive memories. *Neuron* **75**, 133–142 (2012).
- Stujenske, J.M., Likhtik, E., Topiwala, M.A. & Gordon, J.A. Fear and safety engage competing patterns of theta-gamma coupling in the basolateral amygdala. *Neuron* **83**, 919–933 (2014).
- Gabbott, P.L., Warner, T.A., Jays, P.R., Salway, P. & Busby, S.J. Prefrontal cortex in the rat: projections to subcortical autonomic, motor, and limbic centers. *J. Comp. Neurol.* **492**, 145–177 (2005).
- Holstege, G. The periaqueductal gray controls brainstem emotional motor systems including respiration. *Prog. Brain Res.* **209**, 379–405 (2014).
- Subramanian, H.H., Balnave, R.J. & Holstege, G. The midbrain periaqueductal gray control of respiration. *J. Neurosci.* **28**, 12274–12283 (2008).
- Vianna, D.M., Landeira-Fernandez, J. & Brandão, M.L. Dorsolateral and ventral regions of the periaqueductal gray matter are involved in distinct types of fear. *Neurosci. Biobehav. Rev.* **25**, 711–719 (2001).
- Lesting, J. *et al.* Patterns of coupled theta activity in amygdala-hippocampal-prefrontal cortical circuits during fear extinction. *PLoS One* **6**, e21714 (2011).
- Seidenbecher, T., Laxmi, T.R., Stork, O. & Pape, H.C. Amygdalar and hippocampal theta rhythm synchronization during fear memory retrieval. *Science* **301**, 846–850 (2003).
- Yoder, R.M. & Pang, K.C. Involvement of GABAergic and cholinergic medial septal neurons in hippocampal theta rhythm. *Hippocampus* **15**, 381–392 (2005).
- Stark, E. *et al.* Inhibition-induced theta resonance in cortical circuits. *Neuron* **80**, 1263–1276 (2013).
- Siegle, J.H. & Wilson, M.A. Enhancement of encoding and retrieval functions through theta phase-specific manipulation of hippocampus. *eLife* **3**, e03061 (2014).
- Atallah, B.V., Bruns, W., Carandini, M. & Scanziani, M. Parvalbumin-expressing interneurons linearly transform cortical responses to visual stimuli. *Neuron* **73**, 159–170 (2012).
- Nunez, P.L. & Srinivasan, R. *Electric Fields of the Brain: The Neurophysics of EEG* 2nd edn. (Oxford Univ. Press, 2006).
- Magee, J.C. Dendritic integration of excitatory synaptic input. *Nat. Rev. Neurosci.* **1**, 181–190 (2000).
- Vaidya, S.P. & Johnston, D. Temporal synchrony and gamma-to-theta power conversion in the dendrites of CA1 pyramidal neurons. *Nat. Neurosci.* **16**, 1812–1820 (2013).
- Steenland, H.W., Li, X.Y. & Zhuo, M. Predicting aversive events and terminating fear in the mouse anterior cingulate cortex during trace fear conditioning. *J. Neurosci.* **32**, 1082–1095 (2012).
- Goshen, I. *et al.* Dynamics of retrieval strategies for remote memories. *Cell* **147**, 678–689 (2011).
- Ito, J. *et al.* Whisker barrel cortex delta oscillations and gamma power in the awake mouse are linked to respiration. *Nat. Commun.* **5**, 3572 (2014).
- Fujisawa, S. & Buzsáki, G. A 4 Hz oscillation adaptively synchronizes prefrontal, VTA, and hippocampal activities. *Neuron* **72**, 153–165 (2011).

ONLINE METHODS

Animals. Naive male C57BL6/J mice (3 months old, Janvier) and PV-IRES-Cre mice (3 months old, Jackson Laboratory, B6;129P2-*Pvalbtm1^{cre}Arbr/J*) were individually housed for at least 7 d before all experiments, under a 12-h light–dark cycle, and provided with food and water *ad libitum*. Experiments were performed during the light phase. All procedures were performed in accordance with standard ethical guidelines (European Communities Directive 86/60-EEC) and were approved by the committee on Animal Health and Care of Institut National de la Santé et de la Recherche Médicale and French Ministry of Agriculture and Forestry (authorization A3312001).

Behavior. Auditory fear conditioning and testing took place in two different contexts (context A and B). The conditioning and testing boxes were cleaned with 70% ethanol and 1% acetic acid before and after each session, respectively. To score freezing behavior independently of the experimenter, an automated infrared beam detection system located on the bottom of the experimental chambers was used (Coulbourn Instruments). Because the detection of our dependent variable (freezing) was independent of the experimenter, we did not use a blinding process for group allocation or behavior scoring. The animals were considered to be freezing if no movement was detected for 2 s. On day 1, C57BL6/J mice were subjected to a habituation session in context A, in which they received four presentations of the CS⁺ and of the CS⁻ (total CS duration, 30 s; consisting of 50-ms pips at 0.9 Hz repeated 27 times, 2 ms rise and fall, pip frequency, 7.5 kHz, or white-noise, 80 dB sound pressure level).

Discriminative fear conditioning was performed on the same day by pairing the CS⁺ with a US (1 s foot-shock, 0.6 mA, 5 CS⁺–US pairings, inter-trial intervals 20–180 s). The onset of the US coincided with the offset of the CS⁺. The CS⁻ was presented after each CS⁺–US association but was never reinforced (five CS⁻ presentations; inter-trial intervals, 20–180 s). The frequencies used for CS⁺ and CS⁻ were counterbalanced across animals and randomization of CS⁻ and CS⁺ allocation was performed using an online randomization algorithm (<http://www.randomization.com/>).

On day 2, conditioned mice were submitted to a testing session (retrieval session) in context B during which they received 4 and 12 presentations of the CS⁻ and CS⁺, respectively. Thirteen naive C57BL6/J mice recorded simultaneously in the dmPFC and BLA were included in this experiment and the data collected in two distinct replicates. Five additional naive C57BL6/J mice recorded in the vPAG were fear conditioned using the same protocol. Contextual fear conditioning took place in contexts A and B as describe above. On day 1, C57BL6/J mice were subjected for 5 min to a habituation session in context A. Contextual fear conditioning was performed 24 h later by pairing context B with a US. The next day, mice were subjected for 12 min to a testing session (retrieval) in context B. Six naive C57BL6/J mice were included in this experiment and the data collected in two distinct replicates. For neck muscle EMG recordings, C57BL6/J mice were exposed to 20 CS⁺ presentations in context B as describe above and auditory fear conditioning was performed on the same day by pairing the CS⁺ with a US. Seven naive C57BL6/J mice were included in this experiment and the data collected in two distinct replicates.

For optogenetic experiments using channelrhodopsin, PV-IRES-Cre mice and GPF controls were exposed on day 1 to context A as described above. During the session, four blue-light 4-Hz rhythmic analog (2 or 10 mW, 30 s) stimulations were delivered in the dmPFC to activate parvalbumin-expressing interneurons. On days 2 and 3, mice were exposed to the same context as day 1 or to the neutral context B as described above, without any stimulation, respectively. To test for the frequency and structure specificity of the stimulation, other groups of naive PV-IRES-Cre mice were submitted to four blue-light rhythmic analog dmPFC stimulations at different frequencies (1, 8, 10 and 12 Hz, stochastic 4 Hz composed of 2–12 Hz frequency with an average at 4 Hz, 10 mW, 30 s, $n = 6$ mice) or to four blue-light rhythmic analog stimulations at 4 Hz of the motor cortex ($n = 4$ mice) or the BLA ($n = 5$ mice). These five mice infected in the BLA were also submitted to auditory fear conditioning as described above and tested 24 and 48 h later to evaluate the effect of BLA silencing during fear behavior. Randomization of group allocation (Chr2 versus GFP controls) was performed using an online randomization algorithm (<http://www.randomization.com/>).

For pharmacological experiments, C57BL6/J mice were submitted to a fear conditioning paradigm consisting of CS⁺ and US pairings in context A as described above. On days 2, 3 and 4, conditioned mice were tested in context B,

during which they received four presentations of the CS⁺ before muscimol injections (day 2, test 1), 5 min after muscimol injections (day 3, Inac.) and 24 h after muscimol injections (day 4, test 2). Six naive C57BL6/J mice were included in this experiment and the data collected in two distinct replicates.

Surgery and recordings. Mice were anaesthetized with isoflurane (induction 3%, maintenance 1.5%) in O₂. Body temperature was maintained at 37 °C with a temperature controller system (FHC). Mice were secured in a stereotaxic frame and unilaterally implanted in the left dorsomedial prefrontal cortex (dmPFC) with a multi-wire electrode array aimed at the following coordinates: 2.0 mm anterior to the bregma, 0.3 mm lateral to the midline and 0.8 to 1.4 mm ventral to the cortical surface. They were implanted in the left basolateral amygdala (BLA) with a multi-wire electrode array aimed at the following coordinates: 1.7 mm posterior to the bregma, 3 mm lateral to the midline and 4 mm ventral to the cortical surface.

Another group of mice was implanted only in the ventrolateral periaqueductal gray at the following coordinates: –4.30 mm anterior to the bregma, 0.55 mm lateral to the midline and 2.20 mm ventral to the cortical surface. For contextual fear conditioning experiments, mice were implanted only in the dmPFC. For electromyographic (EMG) recording experiments, Teflon-coated stainless steel electrodes (AM Systems) were sutured into the right and left nuchal muscles. Wires were connected to a multi-wire electrode array connector attached to the skull.

For pharmacological experiments, animals were implanted in the dmPFC at the same coordinate as above and in dorsal hippocampus at the following coordinates: 2 mm posterior to bregma, 1.2 mm lateral to midline and 1.2 to 1.4 mm ventral to the cortical surface. The electrodes consisted of 16 individually insulated nichrome wires (13 μ m inner diameter, impedance 30–100 K Ω ; Kanthal) contained in a 26-gauge stainless steel guide cannula. The wires were attached to an 18-pin connector (Omnetics) and two connectors were used for each mouse. All implants were secured using Super-Bond cement (Sun Medical). After surgery, mice were allowed to recover for 7 d and were habituated to handling. Analgesia was applied before and 1 d after surgery (Metacam, Boehringer). Electrodes were connected to a headstage (Plexon) containing 16 unity-gain operational amplifiers. The headstage was connected to a 16-channel preamplifier (gain 100 \times , bandpass filter from 150 Hz to 9 kHz for unit activity; Plexon). Spiking activity was digitized at 40 kHz and bandpass filtered from 250 Hz to 8 kHz, and isolated by time-amplitude window discrimination and template matching using a Multichannel Acquisition Processor system (Plexon). At the conclusion of the experiment, recording sites were marked with electrolytic lesions before perfusion, and electrode tip locations were reconstructed with standard histological techniques.

Single-unit analyses. Single-unit spike sorting was performed using Off-Line Spike Sorter (OFSS, Plexon) for all behavioral sessions. Principal component scores were calculated for unsorted waveforms and plotted in a three-dimensional principal component space; clusters containing similar valid waveforms were manually defined. A group of waveforms were considered to be generated from a single neuron if the waveforms formed a discrete, isolated cluster in the principal component space and did not contain a refractory period less than 1 ms, as assessed using autocorrelogram analyses. To avoid analysis of the same neuron recorded on different channels, we computed cross-correlation histograms. If a target neuron presented a peak of activity at a time that the reference neuron fired, only one of the two neurons was considered for further analysis.

To separate putative inhibitory interneurons from putative excitatory principal neurons, we used an unsupervised clustering algorithm based on Ward's method. In brief, the Euclidian distance was calculated between all neuron pairs on the basis of the three-dimensional space defined by each neuron's average half-spike width (measured from trough to peak), the firing rate and the area under the hyperpolarization phase of the spike. An iterative agglomerative procedure was then used to combine neurons into groups based on the matrix of distances such that the total number of groups was reduced to give the smallest possible increase in within-group sum of squares deviation.

For the detection of interactions between units recorded in the dmPFC and BLA, the spike trains of each simultaneously recorded pair were binned (10 ms bin size), the cross-correlation of the binned histograms was calculated over multiple lags (maximum lag, ± 500 ms) and the peak cross-correlation coefficient for each pair was determined. For the detection of co-firing property for unit pairs,

spike trains were binned as before and the co-firing index was calculated as the ratio of co-occurring (common) spikes to the total number of spikes for the two units. This provides a simple yet direct measure of the co-occurrence of unit spikes on multiple levels of temporal resolution. For the determination of the bin size and the robustness of the method, different bin sizes were tested; they all gave qualitatively similar results. Among those tested, 10 ms was selected because it allows the identification of potentially monosynaptic interactions. To evaluate whether neurons were oscillating at 4 Hz, we used Gabor functions, which are commonly used to fit autocorrelation (AC) histograms of nonstationary rhythmic biological time series such as neuronal spiking activity^{30–32}. Gabor functions are damped sine waves with two components: first, the sine wave frequency (f_0); second, a damping frequency (f_d) that modulates the amplitude of the sine wave. The Gabor functions served as a predicted AC (pAC) that was used to fit the actual AC of the frequencies of interest. We constructed a set of Gabor functions as follows³²:

$$\text{pAC}_{\text{fofd}} = \cos(2\pi x f_0) \times \exp(-Cx^2 f_d)$$

with f_0 and f_d both ranging from 1 to 25 Hz, hence creating 100×100 predicted ACs. The quality of the fit of each predicted AC was then assessed by its correlation (Spearman's ρ) with the actual AC of specific frequency bands (calculated for lags t of 0–500 ms), and this correlation score was plotted for each f_0, f_d pair. Points showing the highest correlation thus represent candidate f_0, f_d pairs capable of predicting oscillations.

Local field potential and EMG analyses. Local field potentials were analyzed using custom-written Matlab programs. Raw LFP traces were filtered between 0.7 Hz and 400 Hz and downsampled to 1 kHz. All signals were filtered using zero-phase-distortion sixth-order Butterworth filters. For phase analyses, the signal was filtered in the desired frequency band (2–6 Hz for the 4-Hz oscillation) and the complex-valued analytic signal was calculated using the Hilbert transform as below.

$$\rho(t)e^{-i\phi(t)}$$

The vector length and the arctangent of the vector angle provide the estimation of the instantaneous amplitude and instantaneous phase of the signal, respectively, at every time point. All analyses were performed during freezing episodes and, where indicated, during subsampled non-freezing epochs. A phase of 0° corresponds to the peak of prefrontal–amygdala oscillations. LFP power spectrum and LFP–LFP coherence estimations were, unless otherwise noted, performed using the multitaper method³³. Briefly, data were multiplied by a set of 2–5 orthogonal taper functions (discrete prolate spheroidal sequences), Fourier transformed using a window size of 2 s and averaged to obtain a direct multitaper spectral estimate.

Signal to noise ratio (SNR) for 4-Hz power was calculated as the ratio of the mean power in the 2–6 Hz band to the mean power outside this band. Because one mouse did not show immobility behavior during habituation, it was excluded from SNR analyses. For coherence analyses, a method based on imaginary coherence was employed³⁴. Imaginary coherence was calculated as

$$\text{iCoh} = \frac{|\text{Im}(\sum_{\text{bins}} S_{xy})|}{\sqrt{\sum_{\text{bins}} S_{xx} \times \sum_{\text{bins}} S_{yy}}}$$

where S_{xy} is the cross-spectrum, S_{xx} and S_{yy} are the auto-spectra and summation takes place over the spectrogram bins corresponding to the quantified state. By keeping the imaginary part of the normalized cross-spectrum, coherence value is weighted inversely proportionally to the time lag between the two signals. Consequently, it is sensitive only to time-lagged signals, whereas the effect of absolutely synchronous signals is eliminated. Given the very synchronous nature of the oscillation examined here and the small phase lag, imaginary coherence is expected to underestimate the strength of the interaction. However, we opted for this conservative variety of coherence analysis to avoid any influence of volume-conducted currents or artifacts that can artificially boost coherence values.

To investigate any potential causal interaction between the oscillations recorded in the two structures, spectrally resolved Granger causality was

calculated for the unfiltered LFP signals. Granger causality is a statistical measure of the predictive power of one variable over another. Linear trends were removed from the LFP signals and signals were normalized before the analysis. For these analyses, the MVGC multivariate Granger causality toolbox³⁵ was used to fit a higher order vector autoregressive model to the processes. Data were tested for stability in time and model order was determined using the Akaike information criterion. To identify directionality and quantify the lag between the two signals in terms of phase and amplitude, a point process was defined consisting of the peaks of the bandpass-filtered LFP signal for each of the two structures. The lag of the peak of the cross-correlation of these point processes identifies the time lag of the oscillation in the two structures and the directionality of their potential interaction. To avoid any potential bias due to phase asymmetry, the same procedure was tested for the troughs, giving identical results. To investigate this relationship throughout the oscillation cycle, the phase of each analytical signal was extracted using the Hilbert transform and the distribution of the phase differences between the two structures was characterized for deviation from uniformity using circular statistics and Monte Carlo simulations. To evaluate the specific role of phase, amplitude and their interplay on the directionality and causality measures for the LFP data, a procedure was devised for the selective perturbation of phase and amplitude of the signals. Signals were converted in the spectral domain using a discrete Fourier transform and the phase (or amplitude) component of the signal was permuted, leaving the amplitude (or phase) intact. The modified signal was converted back to the time domain using the inverse Fourier transform. For the power comodulation analysis, the power profile for each frequency bin in each structure was calculated and the correlation coefficient of every pair was calculated³⁶.

To compare the impact of CS⁺ during freezing on local theta and 4-Hz phase resetting, we used a multitaper analysis of LFP signals for frequencies ranging from 2 to 12 Hz and computed a stimulus-triggered spectrogram. For the CS⁺-triggered theta and 4-Hz phase overlays, signals were filtered in the corresponding range (theta, 8–12 Hz; 4-Hz, 2–6 Hz) and phases were extracted from the analytic signal as described above. To quantify phase stability across all CS⁺ pips during freezing episodes, we calculated the mean resultant length for all time–frequency pairs. To evaluate the predictive value of 4-Hz power for freezing behavior, we used wavelet analysis, which in some instances allows a higher temporal resolution, to quantify the spectral content of the signal for frequencies between 2 and 12 Hz and computed freezing-triggered spectrograms. To evaluate the latency to freeze in response to the CS⁺, individual tone onsets and freezing period onsets for individual mice were binned (100 ms bin size), smoothed and averaged, and cross-correlation analysis was performed on these data taking freezing onset epochs as the reference event (Fig. 1e). In these conditions, negative lags indicate that conditioned stimuli precede freezing events. Statistical significance was evaluated using two different approaches and then combined. We first simulated 1,000 instances of a uniform distribution of freezing episodes and recomputed the cross-correlation analysis. We next shuffled 1,000 times the freezing ISIs of the actual freezing episodes to preserve the first-order statistics of freezing behavior but perturb its relation to CS⁺ and recomputed the cross-correlation analysis. The results of the two analyses were averaged to produce a more robust significance threshold. However, each individual result was not qualitatively and quantitatively different from the final average. One interesting characteristic of the cross-correlation is its oscillatory nature, which is due to the rhythmic repetition of CS⁺ (27 pips delivered at 1.1 Hz) and the tendency of elicited freezing to occur in response to these events (Fig. 1e).

For correlation analyses between freezing behavior and 4-Hz oscillations (Fig. 3d and Supplementary Fig. 2e), we first evaluated the percentage of time individual animals spent frozen during the entire recording session. For 4-Hz quantification, 4-Hz oscillation periods were evaluated as periods of significant 4-Hz SNR, as compared to baseline (a 2-min period before the first CS presentation). 4 Hz expressed as the percentage of total time corresponds to the ratio of the total duration of 4-Hz episodes to the recording session duration. For electromyographic recordings, unilateral EMG signals were band-pass filtered (100–1,000 Hz), rectified and integrated (convolution with 100-ms Gaussian kernel). The ΔEMG signal was calculated as the differential EMG recorded in the left and right nuchal muscle³⁷. The absolute value of ΔEMG was then Z-score transformed and averaged around freezing onsets (–500 ms to 500 ms) occurring during CS⁺ presentation, during both habituation and fear conditioning.

Phase-locking analyses. For phase modulation analysis, the variance-stabilized $\ln(Z)$ ($Z = R^2/n$, R being the resultant length and n the sample size) statistics for the Rayleigh test for uniformity against the von Mises distribution were calculated^{38,39}. To partially account for the sample size bias of the resultant length, only units with at least 100 spikes during freezing behavior were taken into consideration. All results were corroborated using the pairwise phase consistency method, a bias-free estimate of neuronal synchronization based on the average pairwise circular distance

$$D = \frac{2}{N(N-1)} \sum_{i=1}^{N-1} \sum_{j=(i+1)}^N |\theta_i - \theta_j| \bmod \pi$$

with θ_i and θ_j being the phases from two different spikes. This method is analytically equivalent to the squared phase-locking value⁴⁰. To calculate the statistics for each unit, bootstrap analyses and Monte Carlo simulations were performed. In the Monte Carlo simulations, the Y_{sim} value, indicating the expected value for a uniform prior distribution, was calculated for each sample size. Units for which the Y_{unit} exceeded the 95% percentile of the simulated Y_{sim} estimate were considered phase-locked. For the bootstrap statistics, in order to take into account the higher-order statistics of the spike trains, for each unit the inter-spike intervals were shuffled randomly and the potentially nonuniform prior distribution was calculated.

Phases for both dmPFC and BLA spikes were extracted using the dmPFC 4-Hz oscillation phase that exhibits the highest SNR and allows direct comparison of the phase-locking statistics. For the statistical evaluations, before the phase extraction, the prior distribution of phases of the 4-Hz oscillation was examined, and, as is the case for other neuronal slow oscillations, this prior distribution deviated from the uniform distribution. This bias can alter the phase-locking statistics and produce false positives^{38,39}. To account for this potential bias, the phases of the LFPs were transformed using the inverse of the empirical cumulative density function to return a signal with uniform prior distribution. Following this transformation, the spike phases were drawn from a uniform distribution, allowing the application of circular statistics for detecting deviations from uniformity. For normalized averaged phase density analyses, the circular histogram for each neuron was normalized to the maximum and the averaged circular histogram was computed.

Supervised learning algorithms. To establish the predictive value of dmPFC and BLA 4-Hz oscillations for the animal's behavioral state ("freezing" or "not freezing"), we used two distinct machine learning approaches. Specifically, we used the 4-Hz signal-to-noise ratio (SNR) of the two structures as features to train a naive Bayes classifier and a support vector machine (SVM). On the basis of the time-resolved spectral decomposition of the signals (spectrograms), we calculated the mean 4-Hz SNR across three consecutive time bins (with a bin size of 150 ms) and assigned a binary value based on the behavioral state of the animal during the corresponding time (450 ms: freezing = 1; mobility = 0). Each formed SNR–binary value pair constitutes a single data point used as an input to the classifier.

For this analysis, we considered the total duration of the recordings; that is, all time bins were used in this analysis. SVM projects data into a higher dimensional space and estimates a hyperplane that best separates the data points belonging to distinct classes⁴¹. Naive Bayes classifiers assume independence of the probability distributions of the features and classify the test data on the basis of the maximal posterior probability of class assignment⁴². The data set was randomly split into a training data set containing 70% of the data points, which was used to train the classifiers, and a test data set containing the remaining 30% of data points, that was used to test the accuracy of the algorithms. To estimate the stability of the algorithms and confidence intervals of the accuracy and receiver operating characteristics (ROC) curves of the classifiers, we implemented a Monte Carlo procedure whereby the data set was randomly split 1,000 times in mutually exclusive training and test data sets and the algorithms were trained and tested on the respective data sets. The accuracy, defined as

$$\text{accuracy} = \frac{\text{number of true positives} + \text{number of true negatives}}{\text{number of datapoints}}$$

and the area under the curve (AUC) of the ROC curve were used to characterize the performance of the classifiers and were compared with the same algorithms trained on shuffled data using the exact same Monte Carlo procedure.

Statistical analyses. For each statistical analysis provided in the manuscript, the Kolmogorov–Smirnov normality test was first performed on the data to determine whether parametric or non-parametric tests were required. When multiple statistical tests were performed, Bonferroni corrections were applied. Two different approaches were used to calculate the sample size. For studies in which we had sufficient information on response variables, power analyses were carried out to determine the number of mice needed. For studies in which the behavioral effect of the manipulation could not be prespecified, such as optogenetic experiments, we used a sequential stopping rule (SSR). In essence, this method enables null-hypothesis tests to be used in sequential stages by analyzing the data at several experimental points using t -tests. Usually the experiment started by testing only a few animals, and if the P value was below 0.05, the investigator declared the effect significant and stopped testing. If the P value was greater than 0.36, the investigator stopped the experiment and retained the null hypothesis.

For sample-size estimation using power analyses, we used a power analysis calculator (G*Power3). For each analysis, sample size was determined using a power >0.9 and α error = 0.05. All tests were two-sided. Power analyses were computed for matched pairs (cued and contextual fear conditioning protocol (Fig. 1 and Supplementary Fig. 4) and pharmacological experiments (Supplementary Fig. 5)). In our behavioral experiments, a critical parameter is freezing percentage, and the numerical endpoint typically ranged between 50% and 70% freezing for CS⁺ presentations immediately following auditory fear conditioning and between 10% and 30% freezing for CS⁻ presentations. A minimum biologically significant difference in the mean values between CS⁻ and CS⁺ conditions for cued fear conditioning (Fig. 1) or between habituation and test sessions for contextual fear conditioning (Supplementary Fig. 4) is 1.5-fold. If we assume a s.d. of 1.5 for a mean value of 60% freezing for CS⁺ test session and 20% freezing for CS⁻ habituation (which are realistic numbers), then a minimum $n = 6$ is needed to reject the null hypothesis with 90% probability. Sample size determination using SSR analyses was used for optogenetic experiments, in which it was not possible to determine a priori the effect of the optical manipulation. We used P values of 0.05 and 0.36 for the lower and upper criteria.

Muscimol inactivation. Mice were unilaterally implanted with a stainless steel guide cannula (26 gauge; Plastics One) aimed at the medial septum using an angle of 10° and recording electrodes were implanted in the dmPFC and the dorsal hippocampus as described in the section "Surgery and recordings". To target the medial septum, we used the following coordinates: 1 mm anterior to bregma; 0.7 mm lateral to midline and 3.0 to 3.3 mm ventral to the cortical surface with an angle of 10° in the coronal plane. The cannula was secured using Super-Bond cement (Sun Medical). On the injection day, muscimol (muscimol–bodipy–TMR-X conjugate, Invitrogen; 0.8 mM in PBS 0.1 M) was infused at a rate of 0.2 $\mu\text{L}/\text{min}$ over 2 min (total volume of 0.4 μL). On the injection day, muscimol was infused 15 min before the behavioral test. After the end of the experiment, muscimol was again infused with the same parameters to control for drug diffusion in the medial septum and mice were perfused. Brains were collected for histological analyses as described below.

Anatomical analysis. Mice were euthanized with isoflurane and perfused through the left ventricle with 4% w/v paraformaldehyde (PFA) in 0.1 M PBS. Brains were dissected out and postfixed for 24 h at 4 °C in the same solution. 60- μm -thick sections were cut, mounted on gelatin-coated microscope slides and dried. Sections were stained with toluidine blue, dehydrated and mounted. Electrolytic lesions were identified with conventional transmission light microscopy. Only recordings with confirmed lesions in cingulate or prelimbic areas of dmPFC and basolateral amygdala (BLA) were included in our analyses. For verification of muscimol injections in the medial septum and viral injections in dmPFC, BLA or motor cortex, serial 80- μm -thick slices were imaged using an epifluorescence system (Leica DM 5000) fitted with a 10 \times dry objective. The location and the extent of the injections or infections were visually controlled. All included muscimol injections were targeted and limited to the medial septum. Similarly, only infections accurately targeting the region of interest were considered for behavioral and electrophysiological analyses.

Virus injections and optogenetics. For optical identification of parvalbumin-expressing interneurons, conditional AAV encoding ChR2 (AAV-EF1a-DIO-hChR2(H134R)-EYFP, serotype 5, Vector Core, University of North Carolina)

or ArchT (AAV-FLEX-ArchT-GFP, serotype 5, Vector Core, University of North Carolina) were bilaterally injected into the dmPFC of PV-IRES-Cre mice ($n = 12$ mice) from glass pipettes (tip diameter 10–20 μm) connected to a Picospritzer (Parker Hannifin Corporation; approximately 0.4 μL per hemisphere) at the following coordinates: dmPFC: 2.0 mm anterior to bregma, 0.4 mm lateral to midline and 0.9 to 1.2 mm ventral to the cortical surface. One to 2 weeks after the injection, mice were implanted bilaterally with optic fibers (diameter, 200 μm ; numerical aperture, 0.37; flat tip; Doric Lenses) at the same coordinates. All implants were secured using Super-Bond cement (Sun Medical). For experiments using optogenetic stimulation coupled to single-unit and LFP recordings, one of the two optic fibers was combined to the array of 16 or 32 individually insulated nichrome wires. Single-unit recordings during the manipulation of PV interneurons were performed as described in the section “Surgery and recordings.”

Behavioral and recording experiments were performed 3–5 weeks after injection. The light (approximately 2 or 10 mW per implanted fiber) was bilaterally conducted from the laser (OptoDuet 473/593 nm, Ikecool) to the mouse via two fiber-optic patch cords (diameter, 200 μm , Doric Lenses) connected to a rotary joint (1×2 fiber-optic rotary joint, Doric Lenses) that allowed mice to freely move in the behavioral apparatus. For optical control of parvalbumin-expressing interneurons, conditional AAV encoding ChR2 (AAV-EF1a-DIO-hChR2(H134R)-EYFP, serotype 5, Vector Core, University of North Carolina) was bilaterally injected into the dmPFC or the BLA at the same coordinates as above or into the motor cortex of PV-IRES-Cre mice at the following coordinates: 2.0 mm anterior to bregma, 1.5 mm lateral to midline and 1.3 mm ventral to the cortical surface. Control experiments were performed using an AAV containing the DNA construct for GFP alone (AAV-FLEX-GFP, Vector Core, University of North Carolina).

For optogenetic manipulation of PV interneurons during behavior, we used a 30-s analog dmPFC stimulation delivered at 1, 4, 8, 10 or 12 Hz. As a control we also used a stochastic 4-Hz analog dmPFC stimulation generated by an oscillator with a randomly time-modulated frequency drawn from a Gaussian distribution centered on 4 Hz. The power spectrum of the signal displayed a broad peak

around 4 Hz, but the duration of each cycle varied randomly from 0.15 to 0.6 s, thereby destroying the regularity of the population activity. For motor cortex experiments, we used a 4-Hz analog stimulation. For BLA silencing experiments, a continuous pulse of blue light was applied during CS⁺ presentations 24 h after fear conditioning. After behavioral and recording experiments, mice were perfused and histological analysis was performed.

A **Supplementary Methods Checklist** is available.

30. Engel, A.K., König, P., Gray, C.M. & Singer, W. Stimulus-dependent neuronal oscillations in cat visual cortex: inter-columnar interaction as determined by cross-correlation analysis. *Eur. J. Neurosci.* **2**, 588–606 (1990).
31. Gray, C.M., König, P., Engel, A.K. & Singer, W. Oscillatory responses in cat visual cortex exhibit inter-columnar synchronization which reflects global stimulus properties. *Nature* **338**, 334–337 (1989).
32. Young, M.P., Tanaka, K. & Yamane, S. On oscillating neuronal responses in the visual cortex of the monkey. *J. Neurophysiol.* **67**, 1464–1474 (1992).
33. Mitra, P.P. & Pesaran, B. Analysis of dynamic brain imaging data. *Biophys. J.* **76**, 691–708 (1999).
34. Nolte, G. *et al.* Identifying true brain interaction from EEG data using the imaginary part of coherency. *Clin. Neurophysiol.* **115**, 2292–2307 (2004).
35. Barnett, L. & Seth, A.K. The MVGC multivariate Granger causality toolbox: a new approach to Granger-causal inference. *J. Neurosci. Methods* **223**, 50–68 (2014).
36. Buzsáki, G. *et al.* Hippocampal network patterns of activity in the mouse. *Neuroscience* **116**, 201–211 (2003).
37. Steenland, H.W. & Zhuo, M. Neck electromyography is an effective measure of fear behavior. *J. Neurosci. Methods* **177**, 355–360 (2009).
38. Siapas, A.G., Lubenov, E.V. & Wilson, M.A. Prefrontal phase locking to hippocampal theta oscillations. *Neuron* **46**, 141–151 (2005).
39. Sirota, A. *et al.* Entrainment of neocortical neurons and gamma oscillations by the hippocampal theta rhythm. *Neuron* **60**, 683–697 (2008).
40. Vinck, M., van Wingerden, M., Womelsdorf, T., Fries, P. & Pennartz, C.M. The pairwise phase consistency: a bias-free measure of rhythmic neuronal synchronization. *Neuroimage* **51**, 112–122 (2010).
41. Cortes, C. & Vapnik, V. Support-vector networks. *Mach. Learn.* **20**, 273–297 (1995).
42. Bishop, C.M. *Pattern Recognition and Machine Learning* (eds. Jordan, M., Kleinberg J. & Schölkopf, B.) (Springer, 2006).